SHARK-NIR coronagraphic simulations: performance dependence on the Strehl ratio

Carolo, E., Vassallo, D., Farinato, J., Agapito, G., Bergomi, M., et al.

E. Carolo, D. Vassallo, J. Farinato, G. Agapito, M. Bergomi, F. Biondi, S. Chinellato, A. Carlotti, M. De Pascale, M. Dima, V. D'Orazi, D. Greggio, D. Magrin, L. Marafatto, D. Mesa, E. Pinna, E. Portaluri, A. Puglisi, R. Ragazzoni, M. Stangalini, G. Umbriaco, V. Viotto, "SHARK-NIR coronagraphic simulations: performance dependence on the Strehl ratio," Proc. SPIE 10701, Optical and Infrared Interferometry and Imaging VI, 107012B (9 July 2018); doi: 10.1117/12.2312553

SPIE.

Event: SPIE Astronomical Telescopes + Instrumentation, 2018, Austin, Texas, United States

SHARK-NIR coronagraphic simulations: performance dependence on the Strehl Ratio

Carolo E.[a,b], Vassallo D.[a,b], Farinato J.[a,b], Agapito G.[d,b], Bergomi M.[a,b], Biondi F.[a,b], Chinellato S.[a,b], Carlotti A.[c], De Pascale M.[a,b], Dima M.[a,b], D'Orazi V.[a,b], Greggio D.[a,b], Magrin D.[a,b], Marafatto L.[a,b], Mesa D.[a,b], Pinna E.[d,b], Portaluri E.[a,b], Puglisi A.[d,b], Ragazzoni R.[a,b], Stangalini M.[e,b], Umbriaco G.[a,f,b], and Viotto V.[a,b]

[a]INAF - Osservatorio Astronomico di Padova, Vicolo dell'Osservatorio 5, 35122, Padova, Italy
[b]ADONI - Laboratorio Nazionale Ottiche Adattive, National Laboratory for Adaptive Optics, Italy
[c]Institut de Planétologie et d'Astrophysique de Grenoble, 414, Rue de la Piscine, Domaine Universitaire, 38400 St-Martin d'Hères, France
[d]INAF - Osservatorio Astrofisico di Arcetri, Largo Enrico Fermi 5, 50125 Firenze, Italy
[e]INAF - Osservatorio Astronomico di Roma, Via Frascati 33, 00078 Monte Porzio Catone, Roma, Italy
[f]Dipartimento di Fisica e Astronomia, Università degli Studi di Padova, Vicolo dell'Osservatorio 3, 35122, Padova, Italy

ABSTRACT

SHARK-NIR is a coronagraphic camera that will be implemented at the Large Binocular Telescope. SHARK-NIR will offer extreme AO direct imaging capability on a field of view of about 18" x 18", and a simple coronagraphic spectroscopic mode offering spectral resolution ranging from 100 to 700. In order to meet the SHARK-NIR main scientific driver, i.e., searching for giant planets on wide orbits, a high contrast is necessary. A set of coronagraphic masks were tested, we selected the best performing configurations for the instrument: the Gaussian-Lyot coronagraph, a Shaped Pupil (SP) with 360° of discovery space and two SP masks with asymmetric detection area but with a small inner working angle and the Four Quadrant phase mask. Many simulations were performed to obtain the performance in different atmospheric conditions, including seeing variations, by using magnitude guide star from R = 8 to R = 14 and testing also the jitter value. These changes in simulation parameters reflected a variation in the coronagraphic performance. We analysed the simulation images by searching the best post processing to obtain the best performance for the coronagraph, moreover, we have taken account the fact that using, in the ADI technique, small subsets to generate the reference PSF can help attenuating the speckle noise, but it also results in a growing risk of planet removal if not enough field rotation occurs in the subset itself. We analysed the results after this effect is included, so the performances were shown as function of the Strehl Ratio condition to obtain mass and age limits for the detection of the planets.

Keywords: SHARK-NIR, Coronagraphy, Exoplanets, ADI, PCA

1. INTRODUCTION

The detection of exoplanets via direct imaging technique is one of the most exciting goals in modern astrophysics. It provides us with access to information on giant gaseous planets outside the Solar system, that is planets similar to ours Jupiter, Saturn, Uranus and Neptune. A key property of the Large Binocular Telescope (LBT) Adaptive Optic (AO) system is the capability of achieving high Strehl Ratio (SR) at moderately faint magnitude ($R > 10$). The AO refurbishment (SOUL; The Single conjugated adaptive Optics Upgrade for LBT) will provide an additional 1-2 magnitude gain to obtain the same level of correction as given by the First-Light Adaptive

Further author information: (Send correspondence to E.C.)
E.C.: E-mail: elena.carolo@inaf.it

Optical and Infrared Interferometry and Imaging VI, edited by Michelle J. Creech-Eakman, Peter G. Tuthill, Antoine Mérand, Proc. of SPIE Vol. 10701, 107012B · © 2018 SPIE
CCC code: 0277-786X/18/$18 · doi: 10.1117/12.2312553

Optics (FLAO), opening the field of high-contrast AO imaging to stars much fainter than feasible using the Spectro-Polarimetric High-contrast Exoplanet REsearch (SPHERE) and the Gemini Planet Imager (GPI). This feature will allow deep search for planets around targets like, e.g., K/M dwarfs in nearby young associations and/or solar type stars in nearby star-forming regions (e.g., Taurus-Auriga, located at d=140 pc). Furthermore, the Northern hemisphere location implies that the direct competition with SPHERE and GPI is limited to equatorial targets. SHARK may allow detecting planets in formation phase in the well-studied Taurus-Auriga star forming region. This is northern and hence badly accessible with SPHERE and GPI. The bulk of the members have ages of about 1-2 Myr, at a distance of about 140 pc.

2. CORONAGRAPHIC MASKS

Coronagraphy is a very wide field: several techniques have been proposed through years, with a huge effort both theoretical and experimental. A relevant reference in this context is e.g.1. A few different solutions will be finally implemented in SHARK-NIR, thanks to the presence of wheels in all of the three coronagraphich planes. The goal of this study is to converge on a final suite. The final selection is based on the simulated performance. Several factors might influence the performance, with each technique generally behaving differently in response to each of them:

1. Geometry of LBT pupil
2. Vibration environment at LBT
3. Upstream aberrations (AO residual and the Non Common Path Aberration (NCPA))
4. 50 millimeters separation between the position of the first intermediate pupil plane and the apodizers wheel
5. Finite tolerance in the alignment of the apodizer with respect to the telescope pupil
6. PSF stability in the coronagraphic focal plane
7. Chromatism

As a result of a preliminary study, we first narrowed the focus to a small subsample of techniques. There are three planes in SHARK-NIR that can be used for coronagraphy: two pupil planes and one focal plane in-between. All techniques that are not compatible with the opto-mechanics of the instrument are of course immediately discarded. The Lyot concept and its improvements with both amplitude and phase masks are the most suitable options.

2.1 Gaussian-Lyot

In the classical Lyot configuration, amplitude transmission is a simple boxcar function. Several other transmission profiles have been proposed during the years to control diffraction. In a Gaussian Lyot coronagraph, the electric field amplitude in the image plane is spatially modulated according to a Gaussian transmission profile.

2.2 Shaped pupil

As suggested by its name, the Shaped Pupil (SP) technique consists in reshaping the telescope pupil so to generate dark areas in the focal plane via distructive interference. Stricly speaking, shaping here means to constrain transmission to be either 0 or 1 across the pupil (for a review of apodization techniques see e.g. 2). With currently available algorithms, masks can be designed for any arbitrary pupil geometry to generate regions of high contrast in the image plane tailored to any desired shape or size.[3]

2.3 Four-quadrant phase-mask

This coronagraph suppresses on-axis starlight by means of a phase mask in the focal plane. The mask divides the Four Quadrant Phase Mask (FP) into four quadrants and induces a π phase shift on two of them on one diagonal. Provided that the image of the star is perfectly centered on the common vertex of the quadrants, then the four outcoming beams combine destructively at infinity and the stellar light in the downstream pupil plane is totally rejected outside of the pupil area.[4] This light is then easily blocked by means of a Lyot stop. This concept has been tested with near-infrared light both in the lab[5] and on sky.[6] The two major drawbacks of this technique are its high sensitivity to aperture geometry and tip-tilt. The former stems from the fact that the phase mask diffracts light to the outer regions of pupil intensity discontinuities, as central obscurations or support structures. Thus, light is not completely rejected outside the pupil image in presence of these elements, resulting in a contrast degradation proportional to the obscured area. Tip-tilt aberrations cause instead starlight to unfairly breakdown into the four beams, undermining their destructive interference. Despite of this limitations, simulations showed that the FQPM represents an intriguing solution for SHARK-NIR, ensuring a way to further increase the detection capability of the instrument at very small angular separations in the high-SR regime.

3. CORONAGRAPHIC SIMULATION

SHARK-NIR is a coronagraphic camera. Since coronagraphs deal with diffraction of light, it is necessary to operate in the framework of wave-propagation physics: given the mathematical complexity of this theory, the most common approach is to make use of numerical simulations. For the purpose, a Fresnel simulator in IDL language is developed.[7] Starting from the optical design of SHARK-NIR, a simplified 1-D model of the telescope+camera system is developed in the form of an IDL module whose backbone is a sequence of calls to procedures and functions belonging to IDL library PROPER.[8] This module is the very functional core of the simulator: it takes an electric field disturbance and numerically propagates it through the optical train according to scalar theory of diffraction, from the entrance pupil of the system until the detector plane. Intensity in this final plane is then recorded and used to generate the synthetic image. Initial conditions for the disturbance are here represented by the different sources of optical aberrations: residuals from AO correction, NCPA and telescope jitter.

4. DATA PROCESSING

For exoplanets detection, the baseline data-processing algorithm is Angular Differential Imaging (ADI). ADI is a technique routinely used on direct imaging data to suppress the quasi-static structure present in the PSF of the star.[9] The acquisition of a set of images (usually up to a few hundreds) is performed with the instrument rotator turned off. In this way, an hypothetical off-axis source is made to rotate with respect to the star speckle floor, which is in turn static. Image subtraction then strongly attenuates starlight contamination while highly preserving the planet flux. Because of the very small temporal sampling dictated by the AO framerate, simulating more that one hundred seconds of closed-loop operation is very demanding from the computational point of view. ADI observations typically span up to a few hours, in order to maximize field rotation and, as consequence, minimize planet self-cancellation. If ADI is applied based on the real timeline of the simulation, then planet cancellation would be very close to 100% even at very high angular separations from the host star. A solution to the problem is find putting ourselves in the following situation: images in a simulated sequence are not acquired consecutively, but rather they are distributed to cover a lead time sufficiently long for ADI to be applied. Of course, this is quite an unrealistic situation for two main reasons. First, images are acquired at very slow temporal cadence: 100 seconds ideally distributed over one hour means 95% overhead time). Second, the need to dilate the timeline necessarily forces us to assume the atmosphere as highly stable for long times. This is because seeing fluctuations in atmospheric data cubes are very small. However, these two unrealisic aspects somehow go in the opposite direction: in real observations, the additional noise coming from changes in the atmosphere might be partially compensated by the acquisition of a much larger number of frames. In this sense, the performance obtained assuming a short and diluted sequence may not be dramatically different from the one obtained in a more realistic case. According to the new timeline, we associate an hour angle to each frame in the sequence assuming that culmination happens at the midpoint of the observation. For example, if the sequence is made to span one hour, then hour angles are equally distributed between 0.5 and +0.5 hours.

Assuming a declination for the target, parallattic angles can be finally computed from hour angles, to be used to de-rotate images. By changing the declination it is possible to reproduce any desired field rotation. Targets in Taurus-Auriga range in declination from $\sim 18^\circ$ to $\sim 30^\circ$. At the highest of these values, targets are close to zenithal culmination at LBT latitude. This is a very suitable condition for ADI observations because of the large FoV rotation.

The ADI algorithm is structured in three steps:

I. **Subtraction of a reference PSF from each image in the datacube** The reference PSF is extracted directly from the data. The pipeline implements three different variants of the algorithm, differing in the way this operation is performed:

   - **Single-median**: the reference PSF is the same for each image and it is simply the median of the whole sequence (classical ADI).
   - **Multiple-medians**: the sequence is divided into two or more subsets and the single-median subtraction is applied separately for each of them. In this way, reference PSFs are closer in time (and hence more correlated) to the images they are subtracted from. The drawback is the enhanced planet cancellation.
   - **Principal Component Analysis (PCA)**: PCA algorithm is based on a statistical representation of each frame as a linear combination of its principal orthogonal components. These components are estimated by diagonalization of the covariance matrix associated to the signal. Its application has been reported to be very effective particularly by manipulation of the number of principal components to maximize the signal from the planet near its host star.[10] The number of modes used for the PCA analysis is associated to the variance of the corresponding principal component.

II. **De-rotation of image differences** Images are de-rotated to align the fields of view in preparation of the final step. De-rotation is performed according to images parallattic angles. FoV rotation is critical in defining the amount of planet selfcancellation.

III. **Median-combination of de-rotated images** By median-combining the image differences, noise is further attenuated at best by a factor $\sqrt{N}$, where N is the number of images in the sequence.

The baseline for generating the detection limit curves that I will show is an optimization of the ADI data processing in different observing conditions to maximize the SNR at any given angular separation, with 30 images and 90° of FoV rotation.

4.1 Planet light cancellation

Using small subsets to generate the reference PSF can help attenuating the speckle noise, but it also results in a growing risk of planet removal if not enough field rotation has occurred in the subset itself. In general, self-subtraction depends on planet separation from the host star: the drop of its light is bigger at small separations and decreases at large separations. This is due to the fact that the same FoV rotation corresponds to a slower linear motion of the planet at small radial separations from the star with respect to larger separations. This effect results in a subtraction of both speckles and the planet signal near to the star. The amount of self-cancellation is calculated empirically by using probe planets: basically, I apply ADI to a sequence of images containing only planets at different separations from the star. In these images, planets are properly rotated according to parallattic angles. Their residual (post-ADI) signal is then compared to the initial one to generate a cancellation profile. As already pointed out, the amount of cancellation depends on planet angular separation and, at fixed separation, on the ADI variant used and on the overall FoV rotation.[11] Additionally, there is also a somewhat weaker dependence on the number of images in the ADI sequence.

5. SHARK-NIR CORONAGRAPHIC PERFORMANCE

Detection limit curves in several combinations of guide star magnitude, atmospheric seeing and residual jitters have been generated during the design phase. I will not report the results of the whole simulation

campaign, but I will only focus on a few cases. I report instrument performance in few different observing conditions using differential imaging. The processing algorithm is the optimized ADI data processing (see section 4). The baseline for these simulations is 30 images sequences and FoV rotation of $\sim 90°$. A value of 30 nm of residual NCPA is introduced and a residual jitter of 10 mas rms is associated at the FLAO simulation, while for the SOUL ones the jitter simulated is of 3 mas rms. All simulations are monochromatic at the central wavelength of the H-band ($1.6\mu m$). In Figure 1 SR values for both the FLAO and SOUL configurations taken into account the introdution of the residual NCPA and jitter. A contrast of 2×10^5 can be reached at 300 mas in high SR conditions. It should be stressed that performance can be improved by optimizing post-processing.

R	Seeing ['']	FLAO	SOUL
8	0.4	80%	94%
	0.6	77%	91%
	0.8	71%	-
	1.0	63%	-
10	0.4	74%	92%
	0.6	66%	87%
	0.8	54%	85%
12	0.4	68%	88%
	0.6	60%	83%
	0.8	48%	76%
14	0.4	-	77%
	0.6	-	67%
	0.8	-	52%
15	0.4	-	70%
	0.6	-	51%
	0.8	-	31%

Figure 1. SR @$1.6\mu m$ delivered by the AO simulator PASSATA for both FLAO and SOUL configurations as a function of seeing and guide star magnitude, after the introdution of the residual NCPA and jitter

In Figure 2 an example of the application of the optimized data reduction algorithm described in Carolo and Vassallo in prep. The algorithm basically optimize the reference PSF subtraction as a function of angular separation in order to maximize the SNR. The gain in performance is significant, both in high and low SR regime. Using this optimized algorithm, it is possible to reach a 10^5 contrast at 200 mas and less than 5×10^6 at 400 mas, matching thus the scientific requirements for exoplanets.

5.1 Performance at different Strehl conditions

The plot in Figure 4 and Figure 3 show detection limits in high SR regime with all the selected coronagraphs. The target is bright (R = 8 with FLAO system) and seeing excellent (0.4"). Figure 5 reports the same comparison with a lower SR: R = 10 and seeing is 0.6" . Jitter is 10 mas rms with FLAO system and 3 mas rms with SOUL one. Quantitatively, SR are, respectively, 80% and 94% for the bright star cases and 66% in low SR regime. The Gaussian Lyot ($GAUSS_{JH}$) design is not optimized for high SR observation, the IWA is 3 $\lambda \backslash D$ and the coronagraph can operate in both J and H bands, in pupil stabilized mode and field stabilized one. Despite of the limitations due to the high sensitivity of the mask, the simulations showed that FQPM ($FQPM_H$) represents an intriguing solution for SHARK-NIR, ensuring a way to further

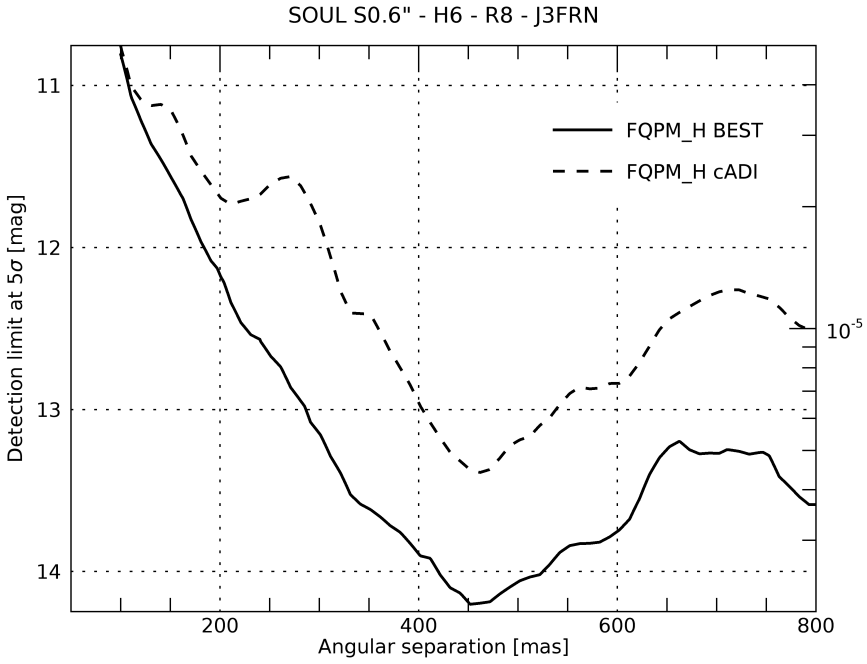

Figure 2. Detection limit in high SR regime with the FQPM obtained with classical ADI compared to the optimized data processing algorithm described in Carolo and Vassallo in prep.

increase the detection capability of the instrument at very small angular separations in the high-SR regime. It allows to access the entire scientific FoV and delivers excellent performance in ideal conditions (high SR), but performance is still good, both close and further away from the star, even at lower SR and with moderate vibrations. The only coronagraph delivering a performance better than the FQPM in limited ranges in high-SR is the Shaped Pupil. $SP1_H$ is intriguing since it is the best one at 130 mas, with half a magnitude gain with respect to phase masks. SP2 (composed by two SPs with complementary discovery space of 120°: $SP2A_H$+$SP2B_H$) is the best coronagraph between 160 and 200 mas from the star.

5.2 Limits on planet mass-age

Using the theorical model AMES-COND[12] we were able to set upper limit on the mass of possible objects around the Taurus-Auriga star forming region. Taurus lies at a mean distance of about 140 pc with a depth of 20 pc or more[13–15] and spans approximately 100 square degrees on the sky, or about a 25 pc diameter at this distance, the bulk of the members have ages of about 1-2 Myr pc. Moreover, we used the detection limit curve obtained by simulating a H magnitudes of 6 for the star, observed by using the FQPM with a high SR condition. The upper mass limit plots obtained in this way are displayed in Figure 6 as solid lines. We found a mass limit of 2.5-6 M_{Jup} at a separation smaller than 20 AU.

6. CONCLUSIONS

After extensive simulation campaigns, the coronagraphic techniques to be implemented in the instrument are selected. In summary, the Gaussian Lyot coronagraph is the option to serve all those science cases requiring field-stabilization and moderate contrast. Observations in pupil-stabilized mode to search for exoplanets can take advantage of two Shaped Pupils and a four-quadrant phase mask coronagraph. The SP are designed for high contrast on a small field close to the star (130 mas) and are robust to image and pupil jitter, while the FQPM allows to access the entire scientific FoV and delivers excellent performance

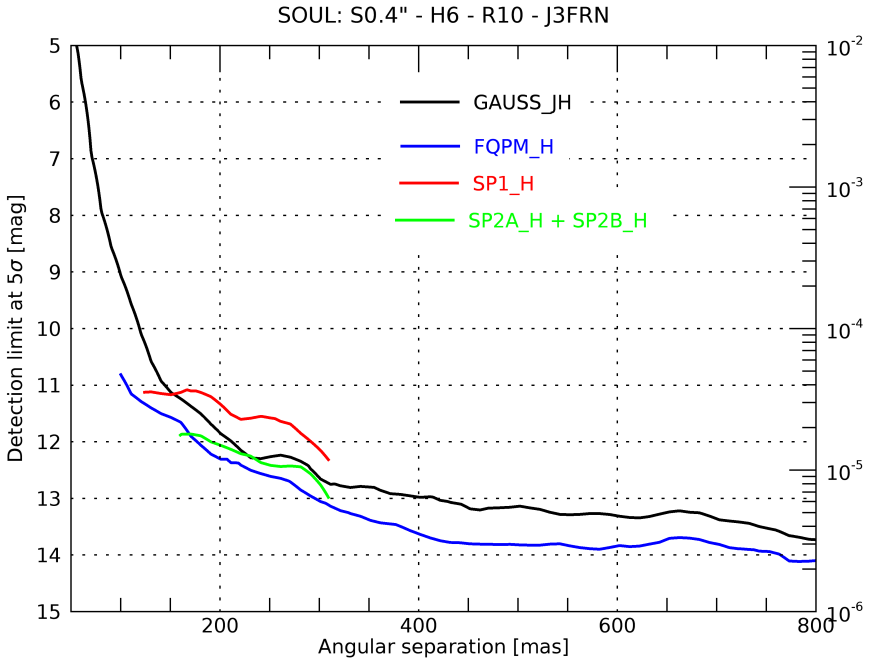

Figure 3. Detection limit in high SR regime for those coronagraphs that have been selected for implementation with SOUL system.

in ideal conditions (high SR), but performance is still good, both close and further away from the star, even at lower SR and with moderate vibrations. Moreover, by using the theorical model AMES-COND[12] we were able to set upper limit on the mass of possible objects around the Taurus-Auriga star forming region we could detect; giant planets of about tens of Jupiter masses.

REFERENCES

[1] Guyon, O., Pluzhnik, E. A., Kuchner, M. J., Collins, B., and Ridgway, S. T., "Theoretical Limits on Extrasolar Terrestrial Planet Detection with Coronagraphs," **167**, 81–99 (Nov. 2006).

[2] Kasdin, N. J., Vanderbei, R. J., Spergel, D. N., and Littman, M. G., "Extrasolar Planet Finding via Optimal Apodized-Pupil and Shaped-Pupil Coronagraphs," **582**, 1147–1161 (Jan. 2003).

[3] Carlotti, A., Vanderbei, R., and Kasdin, N. J., "Optimal pupil apodizations for arbitrary apertures," *ArXiv e-prints* (Aug. 2011).

[4] Rouan, D., Riaud, P., Boccaletti, A., Clénet, Y., and Labeyrie, A., "The Four-Quadrant Phase-Mask Coronagraph. I. Principle," **112**, 1479–1486 (Nov. 2000).

[5] Riaud, P., Boccaletti, A., Baudrand, J., and Rouan, D., "The Four-Quadrant Phase Mask Coronagraph. III. Laboratory Performance," **115**, 712–719 (June 2003).

[6] Boccaletti, A., Riaud, P., Baudoz, P., Baudrand, J., Rouan, D., Gratadour, D., Lacombe, F., and Lagrange, A.-M., "The Four-Quadrant Phase Mask Coronagraph. IV. First Light at the Very Large Telescope," **116**, 1061–1071 (Nov. 2004).

[7] Vassallo, D., Carolo, E., Farinato, J., Bergomi, M., Bonavita, M., Carlotti, A., D'Orazi, V., Greggio, D., Magrin, D., Mesa, D., Pinna, E., Puglisi, A., Stangalini, M., Verinaud, C., and Viotto, V., "An extensive coronagraphic simulation applied to LBT," in [*Modeling, Systems Engineering, and Project Management for Astronomy VI*], **9911**, 99110Y (Aug. 2016).

[8] Krist, J. E., "PROPER: an optical propagation library for IDL," in [*Optical Modeling and Performance Predictions III*], **6675**, 66750P (Sept. 2007).

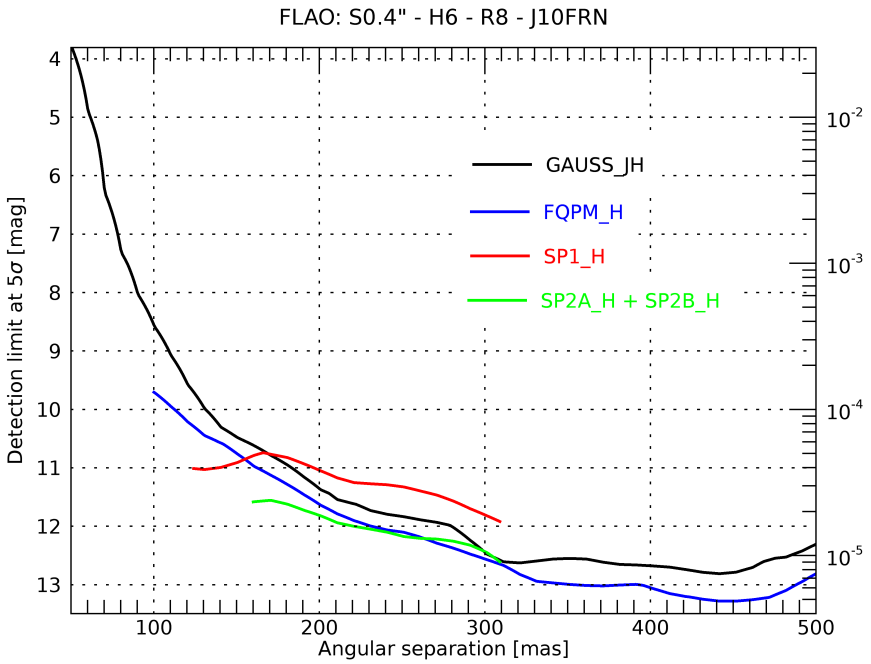

Figure 4. Detection limit in high SR regime for those coronagraphs that have been selected for implementation with FLAO system.

[9] Marois, C., Lafrenière, D., Doyon, R., Macintosh, B., and Nadeau, D., "Angular Differential Imaging: A Powerful High-Contrast Imaging Technique," **641**, 556–564 (Apr. 2006).

[10] Wall, M. E., Rechtsteiner, A., and M., R. L., "Singular Value Decomposition and Principal Component Analysis," *ArXiv Physics e-prints* **http://adsabs.harvard.edu/abs/2002physics...8101W** (2002).

[11] Carolo, E., Vassallo, D., Farinato, J., Bergomi, M., Bonavita, M., Carlotti, A., D'Orazi, V., Greggio, D., Magrin, D., Mesa, D., Pinna, E., Puglisi, A., Stangalini, M., Verinaud, C., and Viotto, V., "A comparison between different coronagraphic data reduction techniques," in [*Adaptive Optics Systems V*], **9909**, 99097Q (July 2016).

[12] Allard, F., Guillot, T., Ludwig, H.-G., Hauschildt, P. H., Schweitzer, A., Alexander, D. R., and Ferguson, J. W., "Model Atmospheres and Spectra: The Role of Dust," in [*Brown Dwarfs*], Martín, E., ed., *IAU Symposium* **211**, 325 (June 2003).

[13] Kenyon, S. J., Dobrzycka, D., and Hartmann, L., "A new optical extinction law and distance estimate for the Taurus-Auriga molecular cloud," **108**, 1872–1880 (Nov. 1994).

[14] Torres, R. M., Loinard, L., Mioduszewski, A. J., and Rodríguez, L. F., "VLBA Determination of the Distance to Nearby Star-forming Regions. II. Hubble 4 and HDE 283572 in Taurus," **671**, 1813–1819 (Dec. 2007).

[15] Torres, R. M., Loinard, L., Mioduszewski, A. J., Boden, A. F., Franco-Hernández, R., Vlemmings, W. H. T., and Rodríguez, L. F., "VLBA Determination of the Distance to nearby Star-forming Regions. V. Dynamical Mass, Distance, and Radio Structure of V773 Tau A," **747**, 18 (Mar. 2012).

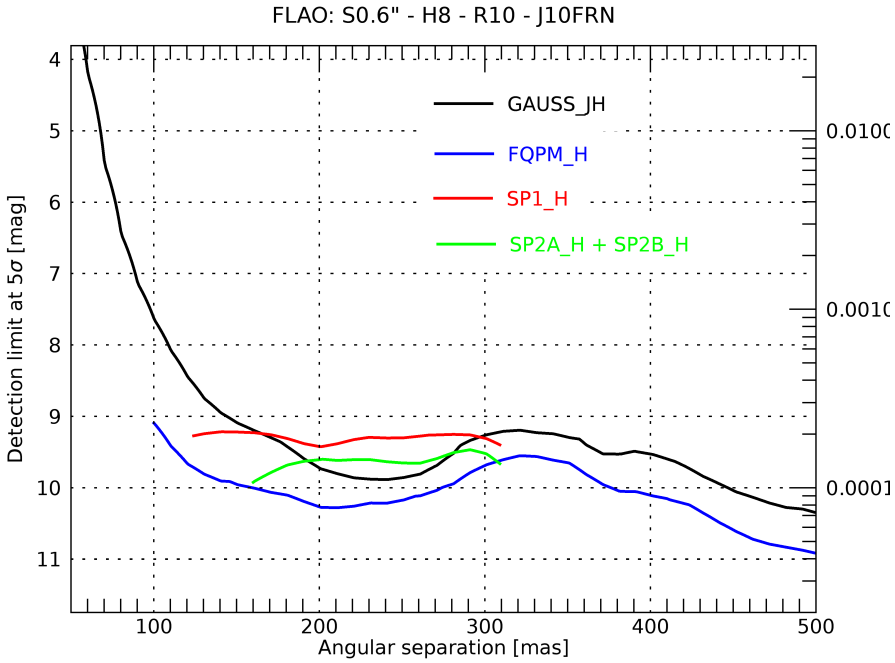

Figure 5. Detection limit in low SR regime for those coronagraphs that have been selected for implementation with FLAO system.

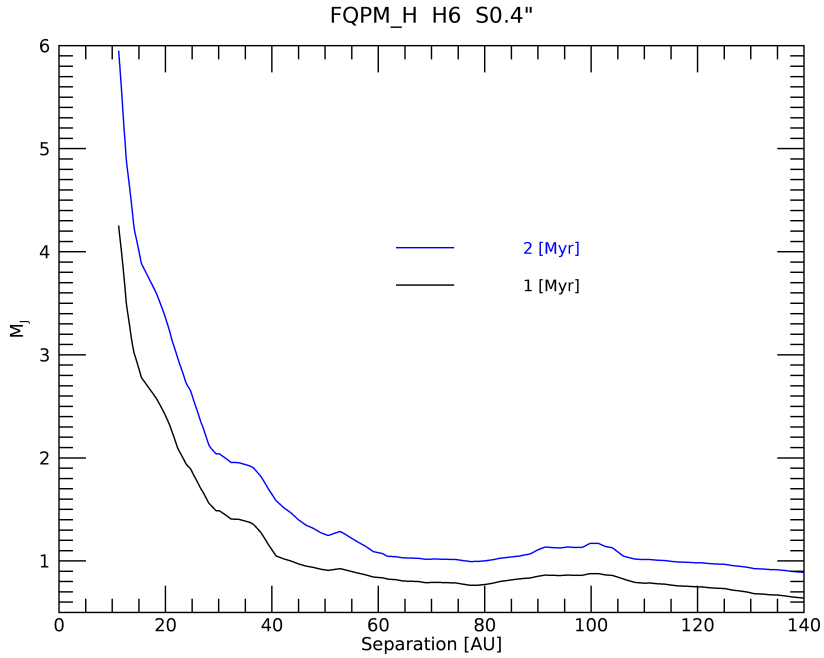

Figure 6. Mass limits for planets around the Taurus-Auriga star forming region calculated from the SHARK-NIR contrast using the AMES-COND model. The solid lines represent limits for a star of 1 and 2 Myr.